Integrated multiplatform method for *in vitro* quantitative assessment of cellular uptake for fluorescent polymer nanoparticles

Raffaele Ferrari[1,6], Monica Lupi[2,6], Francesca Falcetta[2], Paolo Bigini[3], Katia Paolella[3], Fabio Fiordaliso[4], Cinzia Bisighini[4], Mario Salmona[3], Maurizio D'Incalci[2], Massimo Morbidelli[5], Davide Moscatelli[1] and Paolo Ubezio[2]

[1] Department of Chemistry, Materials and Chemical Engineering 'Giulio Natta', Politecnico di Milano, Via Luigi Mancinelli 7, I-20131 Milano, Italy

[2] Department of Oncology, IRCCS—Istituto di Ricerche Farmacologiche Mario Negri, Via La Masa 19, I-20156 Milano, Italy

[3] Department of Biochemistry and Molecular Pharmacology, IRCCS—Istituto di Ricerche Farmacologiche Mario Negri, Via La Masa 19, I-20156 Milano, Italy

[4] Unit of Bio-Imaging, Department of Cardiovascular Research, IRCCS—Istituto di Ricerche Farmacologiche Mario Negri, Via La Masa 19, I-20156 Milan, Italy

[5] Institute for Chemical and Bioengineering, Department of Chemistry and Applied Biosciences, ETH Zurich, Wolfgang-Pauli Strasse 10 8093, Zurich, Switzerland

6 These authors contributed equally to this work.

E-mail: davide.moscatelli@polimi.it

Received 6 September 2013, revised 20 November 2013
Accepted for publication 2 December 2013
Published 7 January 2014

1. Introduction

In the field of polymer drug delivery, the distribution of NPs in cells and organs has a crucial importance in the optimization of the production, structure and functionalization of NPs in terms of their characteristics (e.g. size, ζ potential, etc) [1–3]. Drug delivery studies are often limited by the reliable measurement of the NP distribution in *in vitro* or *in vivo* systems [3]. The presence of polymer NPs in cells and their uptake mechanism is usually tracked by using dyes

physically absorbed into the polymer matrix and the relative fluorescence over time is considered as a measurement of the cell internalization [4, 5]. This approach is somewhat limited because of two main problems, namely the dye release and the impossibility to evaluate the actual number of NPs inside the cells [6, 7]. Furthermore, the formation of NP aggregates and the possible localization of NPs on the cell membrane or inside dead cells represent significant drawbacks that make difficult the exact determination of the NP uptake inside cells. Although these difficulties have been overcome for non-polymer NPs and in particular for gold NPs using mass spectrometric techniques, this is not the case for polymer NPs [7–9].

In this work, a new methodology able to quantify the cellular uptake of NPs has been developed and the validity of this approach has been verified by investigating the internalization of polymer NPs into a tumor cell line, 4T1. Biocompatible poly(methylmethacrylate) (PMMA)-based NPs have been used since they can be traced *in vitro* and *in vivo* over a long period of time without problems due to biodegradation. On the other hand, it is worth noticing that the obtained results provide an important basis for understanding the internalization behavior of biodegradable NPs too, produced through similar processes [10, 11]. PMMA-based NPs are synthesized through an emulsion free-radical polymerization (FRP) process, which ensures a very narrow particle size distribution and a fine control of the final particle size [12]. Fluorescent properties have been added to the NPs by using Rhodamine B (RhB) as a dye. RhB has been linked to a 2-hydroxyethyl methacrylate (HEMA) molecule, making a fluorescent macromonomer functionalized with a vinyl end group, as reported in the literature [13, 14]. This macromonomer has been further copolymerized with MMA in an appropriate and controlled amount, leading to NPs with the same fixed and tunable amount of RhB covalently bonded to the polymer chains. A univocal correlation between fluorescence intensity and number of NPs exists for such fluorescent polymer biocompatible and non-biodegradable NPs. It has in fact been shown that no free RhB molecules have been found in the NP water dispersions. Accordingly, simple and well known relationships can be used to correlate the fluorescence signal to the number of RhB molecules and, knowing the number of RhB molecules linked to each NP, to the number of NPs themselves. Thus, by integrating these measurements with flow cytometric techniques we can evaluate the number of NPs internalized in each cell. Moreover, multiparametric flow cytometry analyses allowed us to discriminate between incorporation into viable and dead cells and to discard signals from free NPs or aggregates of NPs not removed by washing the samples. Finally, the NP uptake and localization into the cells has been qualitatively verified through time-lapse microscopy and confocal microscopy [15, 16].

Other papers consider only flow cytometric measurements together with confocal microscopy, obtaining relative fluorescence values [4, 17, 18], or spectroscopic methods [19, 20], or quantify the number of NPs made with non-polymeric materials [21–23]. The novelty of this work is the development of a robust quantification of the polymer NP uptake through a cross validation of three different techniques: plate-based fluorescence spectroscopy, Coulter counter, and flow cytometry. These analytical techniques have been integrated here, overcoming the intrinsic limitations of each measurement.

2. Methods

2.1. Synthesis of fluorescent NPs

Positively charged PMMA-based NPs with a diameter of 100 nm were synthesized through batch emulsion polymerization (BEP), while negatively charged NPs with a diameter of 100 nm were produced through monomer starved semi-batch emulsion polymerization (MSSEP). BEP and MSSEP have been performed by using respectively 2,2′-azobis(2-methylpropionamidine) dihydrochloride and KPS as initiators. Reactions were carried out adopting Tween 80 as a surfactant in batch and semi-batch conditions using a 100 ml three necked glass flask equipped with a reflux condenser. Temperature was controlled with an external oil bath set to 80 ± 1 °C. Different masses of Tween 80 were added to 100 ml of deionized water and the atmosphere of the reactor was kept inert through vacuum–nitrogen cycles. After that, for BEP reaction, MMA, in which an appropriate amount of fluorescent macromonomer (HEMA-RhB) had been previously dissolved (0.1% w/w), was injected into the purged system with a syringe. The system was maintained under magnetic stirring at 350 rpm. Finally, 0.08 g of the proper initiator were added to initiate the reaction. For MSSEP reaction the solution of the two monomers was injected into the system with a flow rate of 3 ml h^{-1} using a syringe pump (model NE-300, New Era Pump System, Farmingdale, US) after the initiator injection in the purged solution. The reaction was run for three hours; final monomer conversion has been measured through gravimetric measurement and calculated as higher than 99.5%. After the synthesis, the pH was adjusted to 7 using 0.1 M NaOH. Detailed synthesis and characterization of both fluorescent macromonomer and NPs characterized by different sizes, surface charges and amounts of fluorescent macromonomer adopted are reported in the supporting information (SI available at stacks.iop.org/Nano/25/045102/mmedia).

2.2. Cellular uptake of NPs

4T1 cells were seeded in six-well plates at the concentration of 10 000 cells ml^{-1}. 24 h after seeding cells were incubated with different NP concentrations. As NPs were suspended in water in the stock, NPs were diluted in culture medium before use (at least 1:10) and control samples were incubated with the highest amount of water used for NP labeling suspension. At the end of the incubation time (2–48 h) with NPs, cells were harvested and cell suspensions were split in three aliquots, for absolute count, plate fluorimetry and flow cytometry measures.

At least three replicated wells were used for each concentration and time in all experiments.

2.3. Analysis of NP fluorescence with microplate reader

NP colloidal suspensions of different concentrations were obtained with twofold serial dilution in PBS, and 300 μl/well of suspension was put in triplicate into a 96-well plate for microplate reader analysis of fluorescence signals. The analysis of fluorescence signals was performed using a multimode microplate reader Infinite® M200 (TECAN, Switzerland) with the following instrumental setting: λ_{exc} 530 nm, λ_{em} 585 nm and gain 100. Instrument response was checked before each experiment and was reproducible within 2% error. The fluorescence signal detected by the instrument was plotted as a function of the number of RhB molecules in each well, derived considering the concentration in the batches (table S-1 available at stacks.iop.org/Nano/25/045102/mmedia) and the dilutions applied. Fluorescence was proportional to bonded RhB and to number of NPs, and from the linear fit of the data we derived the quantity of RhB (pmol) or number of NPs corresponding to a fluorescence unit detected by the microplate reader in the fixed instrumental setting (figure S-5 available at stacks.iop.org/Nano/25/045102/mmedia). The analysis of cell fluorescence after NP labeling was performed putting 300 μl/well of the cell solution prepared for flow cytometric analysis in triplicate in a 96-well plate for microplate reader analysis of fluorescence signals, keeping the instrumental setting and maintaining the same conditions (temperature, pH etc) as used for calibration procedures. The equivalence of the fluorescence signals with and without cells has been verified (figure S-6 available at stacks.iop.org/Nano/25/045102/mmedia).

2.4. Flow cytometric analysis of NP uptake

Cells exposed to NPs were detached, centrifuged at 1200 rpm for 10 min and then resuspended in cold PBS for flow cytometric analysis. We analyzed three replicated samples for each concentration and for each batch of NPs at each time. All the samples were kept on ice before cell acquisition. Flow cytometric analysis was performed using a FACSCalibur flow cytometer (Becton Dickinson, USA) and acquiring at least 5000 events in the region of interest (ROI) including cell events. RhB was excited using an argon laser (λ_{exc}: 488 nm) and its fluorescence was detected in the fluorescence channel FL2 (585/42 nm) using a logarithmic amplifier. Although excitation was not optimal for RhB detection, cellular fluorescence intensity was always at least three times higher than cellular autofluorescence in the absence of NPs. Availability of a laser excitation nearer to the RhB excitation maximum (530 nm) is expected to lower the detection limit. Dead cells were excluded from the analysis by propidium iodide (PI) staining. For this purpose 1 μg ml^{-1} PI in PBS was added to cell suspensions 5 min before flow cytometric analysis. Cells could be divided into different populations: PI impermeable (viable) and PI permeable (dead cells). PI fluorescence (λ_{exc}: 488 nm) was detected in the fluorescence channel FL3 (>670 nm) using a logarithmic amplifier [8]. Despite the partial overlap of PI and RhB fluorescence emissions, correlated detection of FL2 and FL3 enabled a clear separation of signals of dead from viable cells. All samples were run with and without PI to assure the correct positioning of the ROI for dead cells.

2.5. Live-cell time-lapse imaging of NPs uptake

4T1 cells were seeded in a μ-Slide with eight wells for immunofluorescence (ibidi, Germany). 24 h after seeding, NPs were added and the time-lapse measure started. Image capture was controlled by cellˆR software (Olympus, Germany), collecting all images in phase contrast and red fluorescence (λ_{exc}: 572/23 nm, λ_{em}: 628/28 nm) with a UPlanFLN 40× (Ph2) objective. Sequences were captured over 2 h, every 2 min, and for one field for each well. The cellˆR Imaging Station (Olympus, Germany) used for the time-lapse experiment consisted of an IX81 motorized inverted microscope (Olympus), an incubator (Okolab, Italy) to maintain optimal environmental conditions for cell growth—control of temperature, humidity and CO_2, an MT20 illumination system, equipped with a 150 W Xe arc burner, an ORCA-ER CCD camera (Hamamatsu, Japan) and an X–Y positioning stage.

2.6. Confocal microscopy

For the detection of subcellular localization of NPs, 4T1 cells were seeded at a density of 10 000 cells cm^{-2} into 16 mm diameter well plates on glass cover slips pre-coated with poly-L-lysine. 24 h after seeding, cells were labeled with NPs at the following concentrations: for 50 and 100 nm NPs 2×10^{11} NPs ml^{-1}; for 200− NPs 0.5×10^{11} NPs ml^{-1} and for 200+ NPs 0.25×10^{11} NPs ml^{-1}. The experiments were carried out in triplicate; for each experimental condition, three additional slides without NPs were added as control. At the end of the incubation, cells were fixed with 4% paraformaldehyde in 0.1 M PBS (pH 7.4) and then the nuclear dye Hoechst 33258 (2 μg ml^{-1}, Sigma Aldrich) was added for 45 min. Darkfield images were captured by a CCD camera connected to an Olympus FluoView BX61 microscope coupled to the microscope camera with an FV500 confocal system equipped by specific lasers, $\lambda_{exc} = 405$ nm and $\lambda_{exc} = 546$ nm to visualize Hoechst 33258 and RhB, respectively. All confocal acquisition parameters, including laser settings, are kept constant throughout the acquisition of images. This approach allowed us to compare the signal associated with RhB among the different experimental conditions. In addition, the merge between the fluorescent signal and the images of phase contrast analysis was performed, using an epifluorescence microscope (Olympus BX51 equipped with CCD camera and Olympus-DB software).

3. Results and discussion

3.1. Nanoparticle production

In this work the development of a methodology to assess cellular uptake of nanoparticles in live cells is reported. The

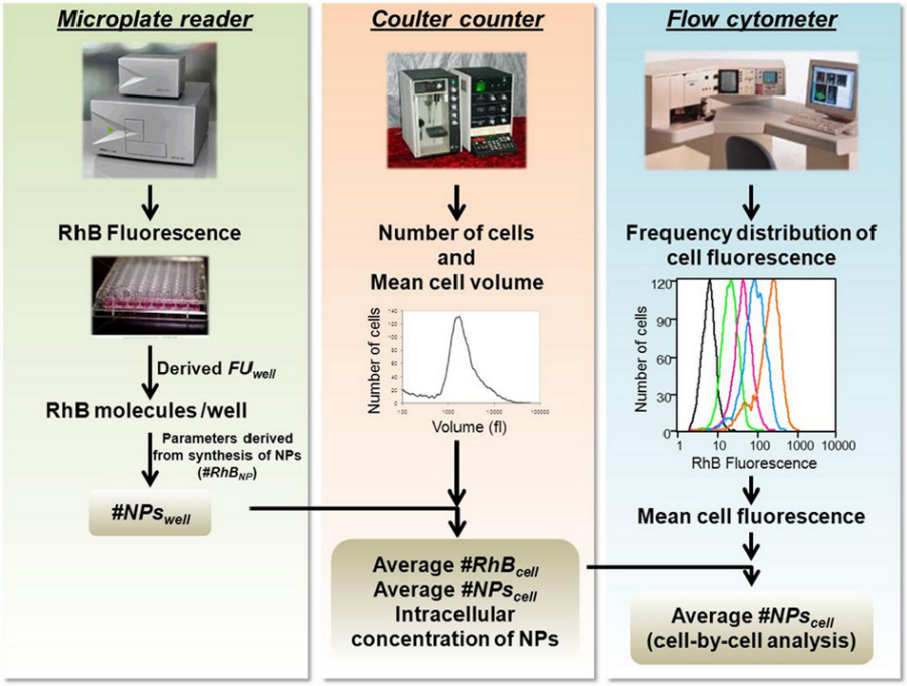

Figure 1. Schematic representation of the adopted experimental procedure.

effectiveness of the proposed methodology has been assessed adopting PMMA-based NPs. These NPs were selected first of all since they are biocompatible and also because they can be synthesized through an emulsion FRP process, by which it is relatively easy to tune the characteristics of the final NPs by changing process parameters such as the amount of emulsifier, the reaction temperature, and the feeding mode [12, 24]. Moreover, this technique permits the synthesis of polymer NPs with narrow particle size distribution (PSD). NPs with different characteristics such as size, surface charge and concentration (table S-1 available at stacks.iop.org/Nano/25/045102/mmedia) have been compared, exploiting the capability of the new methodology.

3.2. Multiplatform analysis of NP uptake

As shown in figure 1, our approach to measure cellular uptake of NPs in living cells involved three independent analytical techniques, each providing a specific piece of information.

In a typical experiment, cells were incubated with a known NP concentration for the desired interval of time, then harvested, centrifuged, resuspended in PBS and split into three samples for fluorescence, Coulter counter and flow cytometric measures. As the culture medium containing free NPs was discarded, the microplate reader (figure 1—left column) measured the overall fluorescence (FU_{well}) generated only by RhB fluorescence of NPs associated with the cells put into each well, in arbitrary fluorescence units, FU_{well}. The first necessary step towards the quantification of internalized NPs is the calibration of the response of the microplate reader for each NP type. This was done using a calibration scale for RhB–NPs obtained with serial dilutions of NPs with known RhB concentration (or NP concentration, see table S-1 available at stacks.iop.org/Nano/25/045102/mmedia) as described in detail in section 2. This calibration, independently obtained for each type of NP, was always strictly linear (figure S-5 available at stacks.iop.org/Nano/25/045102/mmedia) and enabled us to convert the FU_{well} into the number of molecules of RhB per well ($\#RhB_{well}$) or of NPs per well ($\#NPs_{well}$). In order to test whether different environmental conditions could affect the calibration of the microplate reader, we analyzed serial dilutions of negatively charged NPs with a diameter of 100 nm in different media and at several temperatures, and both in PBS and in cell suspension with two different cell concentrations (figure S-6(a) available at stacks.iop.org/Nano/25/045102/mmedia). The linearity of the signal was always maintained with a minimal variation in the slope of the curve, assuring that the quantification of the average number of NPs per cell could be only marginally affected by the different environmental conditions when the calibration is made in the same conditions (figure S-6(b) available at stacks.iop.org/Nano/25/045102/mmedia). Moreover, the fluorescence signal from internalized NPs did not change after disruption of the cells with detergent. All these data indicate that the fluorescence yield of NP-embedded RhB molecules was poorly sensitive to the cell environment outside the NPs. This was also confirmed by the finding that the slopes of the FU_{well}–$\#RhB_{well}$ relationships were similar in all kinds of NP we tested which share the same PMMA material. Notice that, in the case of the FU_{well}–$\#NPs_{well}$ relationships, instead, the slopes obviously depend on the different number of RhB molecules bonded per NP ($\#RhB_{NP}$, reported in table S-1 available at stacks.iop.org/Nano/25/045102/mmedia).

The cell concentration in each well was directly measured in parallel with the Coulter counter (figure 1—central

column). From the obtained values we derived the number of cells in each well ($\#cells_{well}$), which produced the fluorescence signal detected by the microplate reader. This enabled us to calculate the average number of RhB molecules per cell as

$$\#RhB_{cell} = \frac{\#RhB_{well}}{\#cells_{well}} \quad (1)$$

and the average number of NPs per cell as

$$\#NPs_{cell} = \frac{\#NPs_{well}}{\#cells_{well}} = \frac{\#RhB_{cell}}{\#RhB_{NP}}. \quad (2)$$

It is worth mentioning that the so determined $\#NPs_{cell}$ could in some instances overestimate the actual NP uptake into cells when free NPs or aggregates of NPs are not eliminated by washing the cells, when a non-negligible number of NPs is attached to the external membrane of viable cells, or in the presence of NPs diffused into or attached to dead cells. In order to obtain the correct number of NPs inside the cell, data obtained by the microplate reader on the basis of the overall fluorescence detected for each well were associated with results from a cell-by-cell analysis using flow cytometry in the same sample (figure 1—right column), while confocal microscopy analysis allowed us to localize the NPs inside the cell membrane. Flow cytometry gives as output the frequency distribution of cellular fluorescence within the cell population under examination, thus providing additional valuable information on inter-cell variability of cellular uptake, and it is not affected by extracellular fluorescence due to its cell-by-cell detection system. On the other hand, the flow cytometric fluorescence scale (arbitrary fluorescence units, FU) needs to be calibrated to reach a quantitative estimation of the number of internalized NPs. For this purpose, the average cell fluorescence obtained through flow cytometry was compared to $\#RhB_{cell}$, measured above with plate fluorimetry. By plotting together the data obtained using different NP concentrations of all NP types under optimal conditions (i.e. with negligible dead cells or NP aggregates), we observed a strong linearity between plate fluorimetry and flow cytometry measurements (figure 2).

This provided a strong cross validation of the measures and of the procedure itself. As a consequence, the flow cytometric cell fluorescence scale can be converted into the absolute numbers of RhB molecules per cell, and then into the number of NPs per cell, using the $\#RhB_{NP}$ specific for each NP type. Notice that flow cytometric measures were more precise (mean coefficient of variation, CV, 3%, and lower than 5% in 85% of measures) than microplate reader measures (mean CV 15%, and lower than 20% in 85% of measures). The detection limit of the measure of the mean cell fluorescence in flow cytometry, assumed to be ten standard deviations above the mean cell autofluorescence, was 8.2×10^4 $\#RhB_{cell}$, equivalent to 830 positively charged NPs with a diameter of 50 nm, 120 NPs for 100 nm or 16 NPs for 200 nm (similar values holding in negatively charged NPs). It is important to notice that the use of an apparatus with excitation lines closer to the maximum of RhB excitation is expected to improve sensitivity.

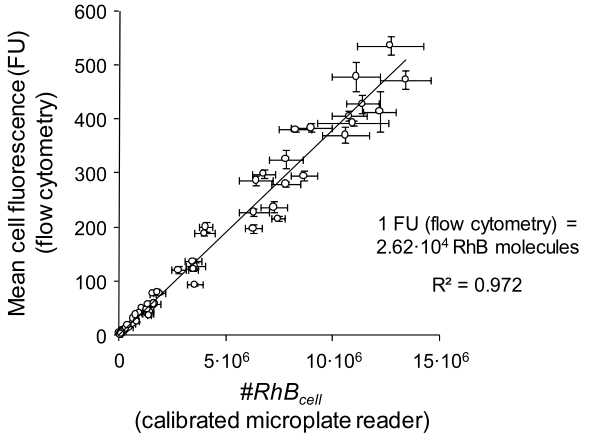

Figure 2. Correlation between mean cell fluorescence detected by flow cytometric analysis (FU) and the number of molecules of RhB per cell obtained by the calibrated microplate reader. All the experimental data from samples labeled with different kinds of NP at several concentrations after 24 or 48 h of incubation were considered together in this plot. Each point represents the mean of three replicates and error bars their standard deviations.

The calibration of the flow cytometric fluorescence scale into absolute numbers of RhB molecules or NPs per cell allowed us to exploit the additional features of this technique for quantitative measures of NP uptake. Flow cytometry gives frequency distributions of cell fluorescence, measuring thousands of cells per minute, easily providing a statistically representative sampling of the heterogeneity of the uptake within the cell population under examination and a detection of subpopulations characterized by different NP uptakes. These subpopulations can also be physically sorted out for further differential analyses. In addition, exploiting the flow cytometry capability for multiparametric analyses, it becomes feasible to correlate directly NP uptake with other parameters of interest on a cell-by-cell basis. Specifically, multiparametric flow cytometry allows the discrimination between signals from viable and dead cells. Figure 3(a) shows a biparametric analysis where NP uptake was measured separately in viable and dead cells, the latter being characterized by incorporation of the fluorescent DNA probe PI, unable to enter viable cells. By acquiring simultaneously fluorescence signals in the 'red' (FL3) and 'orange' (FL2) detection channels, it is possible to measure NP uptake in viable cells only, excluding dead cells on the basis of a higher FL3 signal (figure 3(a) right panel).

The comparison of the frequency histograms of RhB fluorescence before and after PI addition (figure 3(a) lower panel) reveals that the smaller peak observed in the whole population (black line) was produced by dead cells and disappeared in the distribution of viable cells (gray line).

Biparametric flow cytometric analysis of RhB fluorescence (FL2) and side scatter (SSC) (figure 3(b)) revealed the presence of contaminants in some samples, due to free NPs or NPs aggregates, that could not be discarded even by washing the cells. These contaminants produce SSC signals at least one order of magnitude lower than cells; for this reason, all the flow cytometric measures of cellular uptake

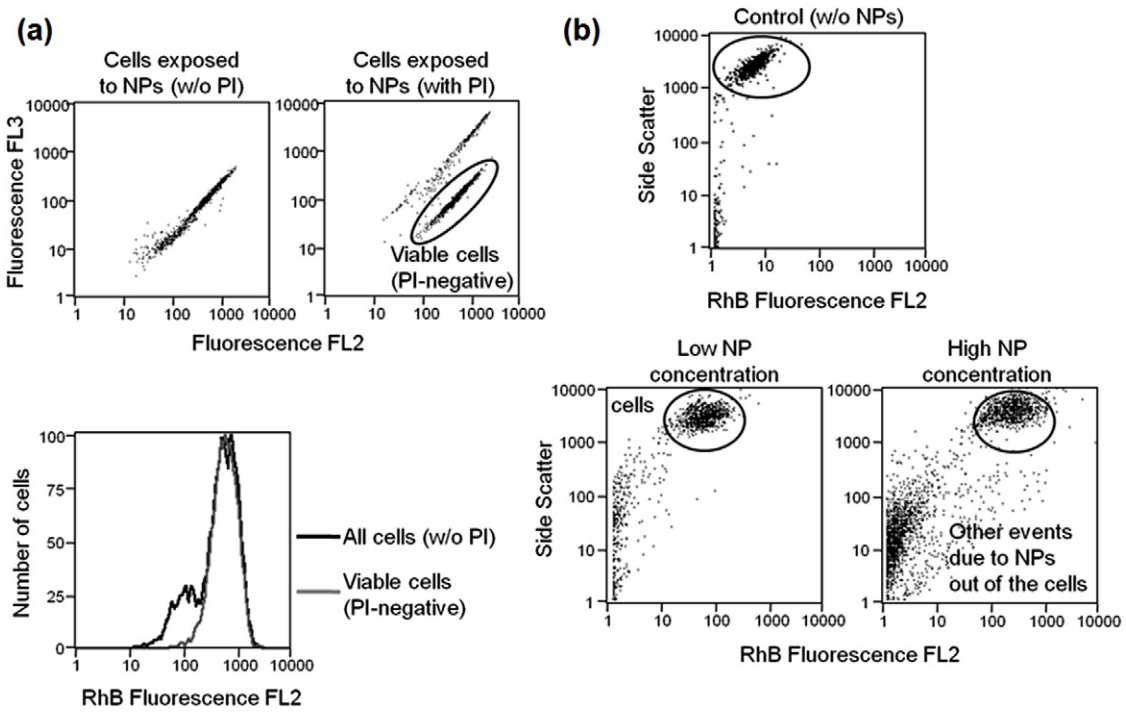

Figure 3. Analysis of cell subpopulations through flow cytometry. (a) Biparametric distribution of FL3 (>670 nm) versus FL2 (585/42 nm) fluorescence. The relative contributions of RhB and PI fluorescence in the FL3 and FL2 channels were different, enabling us to distinguish viable cells (in the elliptic ROI) from PI-permeable cells, which differentially increased the FL3 signal after PI addition, while living cells excluded PI, maintaining the RhB fluorochrome only. In the lower plot we compared the monoparametric distribution of RhB-specific fluorescence (FL2) in the overall population without PI (black line) and among viable cells in the presence of PI (gray line).
(b) Biparametric distribution of side scatter versus RhB fluorescence of control cells, samples exposed to low and high NP concentration. This analysis allowed us to distinguish fluorescence signals from the cells (events highlighted by the elliptic ROI) from those originating from other detected events due to the presence of residual non-internalized NPs. Detection thresholds were purposely kept very low to emphasize the presence of residual NPs.

were made selecting events on the basis of SSC characteristics of the cells, previously set with cell samples not exposed to NPs. As the presence of free NPs can contribute to a wrong estimation of the number of internalized NPs calculated by the microplate reader, samples with non-negligible amounts of such contaminants in a first instance should not be used for calibration. However, if the contamination is unavoidable in calibration samples, a correction of the microplate reader signal is required, and it is feasible using flow cytometry biparametric SSC–RhB fluorescence distributions to assess the contributions of NPs inside and outside the cells. For this purpose, we calculated the fraction of fluorescence generated by the cells with respect to the overall signal using the following formula:

$$\frac{N_{\text{cell}}\overline{\text{FlRhB}}_{\text{cell}}}{N_{\text{tot}}\overline{\text{FlRhB}}_{\text{tot}}} \tag{3}$$

where N_{cell} is the number of events acquired in the elliptic ROI drawn in the FL2–SSC plot (see figure 3(b)), $\overline{\text{FlRhB}}_{\text{cell}}$ is the mean RhB fluorescence of the same region, N_{tot} is the total number of the events acquired and $\overline{\text{FlRhB}}_{\text{tot}}$ is their mean fluorescence. Thus, when the contribution of NPs outside the cells is non-negligible, it is possible to obtain a better estimation of the cellular fluorescence applying the correction factor given by equation (3) to microplate reader measures. In our experiments, dealing with very high NP concentrations in some cell preparations, the correction was tested and enabled these samples to fall on the expected linear relationship (figure 2) between flow cytometry and microplate reader signal.

Another potential pitfall, in this case affecting also the flow cytometric measure, is given by a potential contribution of outside NPs adherent to the cell surface, that would be undistinguishable from the internalized ones. In order to assess the relative importance of these two contributions, we performed confocal microscopy analyses, which in addition allowed us to obtain a detailed picture of the NP intracellular localization (figure 4).

Figure 4(a) shows a representative control sample, with nuclear blue staining and no red signal in the absence of NPs. Figures 4(b) and (c) show the localization in 4T1 cells of negatively and positively charged 100 nm NPs, respectively. The overlapping of fluorescence and phase contrast images (right panels) confirms that both types of NP localize inside the cells in the perinuclear region. Nuclear staining with Hoechst 33258 allowed us to confirm the presence of NPs on the same plane of the nucleus inside the cell volume and to exclude their presence in the nucleus itself; since no RhB fluorescence was detected near the cell membrane, the contribution of external NPs attached to the membrane was proved to be negligible (similar results were obtained for

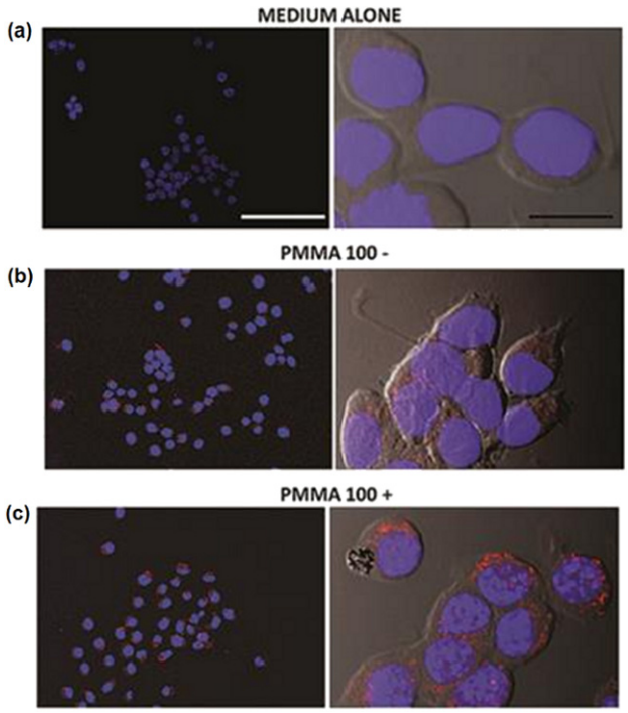

Figure 4. Representative picture of 4T1 cells incubated for 24 h with (a) medium alone, (b) 100 nm negatively charged NPs (100−) and (c) 100 nm positively charged NPs (100+). For each part the left panel corresponds to the overlapping of the signals associated with laser wavelengths λ_{exc} of 405 nm and 546 nm, respectively. The right panel represents the merge between blue/red signals with the contrast phase acquisition. Scale bar: left panels 80 μm; right panels 20 μm.

NPs with different size, as reported in figure S-7, available at stacks.iop.org/Nano/25/045102/mmedia).

3.3. Kinetics of NP internalization and exit

The method was successfully applied to evaluate quantitatively and compare the cellular uptake of polymeric NPs with different sizes (50, 100, 200 nm), surface charges and number of bonded RhB molecules (see table S-1 available at stacks.iop.org/Nano/25/045102/mmedia for $\#RhB_{NP}$ values).

In a first experiment, 4T1 cells were incubated for 24 h with different concentrations for each type of NP. At the end of the incubation time, cells were harvested, washed, counted by Coulter counter and analyzed in parallel by plate microfluorimetry and flow cytometry. Flow cytometric fluorescence distributions of viable cells were unimodal, shifting towards higher fluorescence intensity as NPs concentration increased (figure S-8 available at stacks.iop.org/Nano/25/045102/mmedia), highlighting the concentration dependence of cellular uptake for all kinds of NP. This indicates that all cells in a sample internalized NPs, although to a different extent, spanning over more than one order of magnitude. Flow cytometric histograms were processed and cellular fluorescence first converted to the $\#RhB_{cell}$ with the calibration shown in figure 2 then to $\#NPs_{cell}$ as described above. The results obtained by this quantitative analysis of flow cytometric data have been expressed in terms of the mean absolute number of NPs that were internalized in each cell (figure 5(a)).

These data are in agreement with those previously reported for gold NPs [8] and polymersomes [21], and in particular we found that a higher number of positively charged NPs compared to the negative ones are internalized at the same exposure concentration (figure 5(a)). This difference was considerable for 100 and 200 nm NPs, and smaller for 50 nm NPs, indicating that different mechanisms of internalization were involved for smaller NPs [25, 26]. Comparing the samples exposed at the same concentration of NPs, it is seen that the largest number of internalized NPs was reached for the 50 nm NPs, for both positively and negatively charged materials. However, in terms of the percentage of NPs internalized at 24 h with respect to number of NPs added, this was near 2% in 100 and 200 nm positively charged NPs, 1.4% in positively and 0.7% in negatively charged 50 nm NPs, and one order lower (0.06–0.1%) in 100 and 200 nm negatively charged NPs.

Two NP concentrations, producing detectable fluorescence levels, were chosen for each kind of NP to study the kinetics of the internalization process (figure 5(b)). The fluorescence signal was already close to the maximum after 2 h of incubation, indicating a very fast internalization process, that reached its maximum at about 5 h and then slightly decreased to a sort of equilibrium concentration, with the number of internalized NPs remaining constant over 24 h. This behavior suggests that the uptake process reached an equilibrium where NPs were continuously internalized to compensate the ones that exit and/or NP dilution following cell division, due to sharing of the NPs between mother and daughter cells [4, 8, 27]. Moreover, very short times of incubation were investigated by time-lapse microscopy (figure S-10 available at stacks.iop.org/Nano/25/045102/mmedia). A few minutes after NP addition, the fluorescence signal was already well detectable and localized around the perinuclear region of the cells. Then, fluorescence intensity was rapidly increasing. In a qualitative way, these data fill the gap between the beginning of NP incubation and the first flow cytometric datum, confirming the hypothesis of a very fast internalization process inside the cells [17].

The uptake study was then completed by evaluating NP efflux. For this purpose, 4T1 cells were incubated for 24 h with the previously considered NP concentrations and then left for 24 h in NP-free medium. The results are shown in figure S-9 (available at stacks.iop.org/Nano/25/045102/mmedia) in terms of percentage of NPs retained at the end of the washout process. To take into account cell proliferation, we compared the total number of internalized NPs by multiplying the mean $\#NPs_{cell}$ by the number of cells at 24 and 48 h, i.e. before and after washout. We found that all negatively charged and the 50 nm positively charged NPs were removed from cells, with only about 30% of NPs remaining after 48 h, i.e. 24 h after NP washout. On the other hand, the 100 and 200 nm positively charged ones were more stably internalized, with 80% of NPs still present at 48 h.

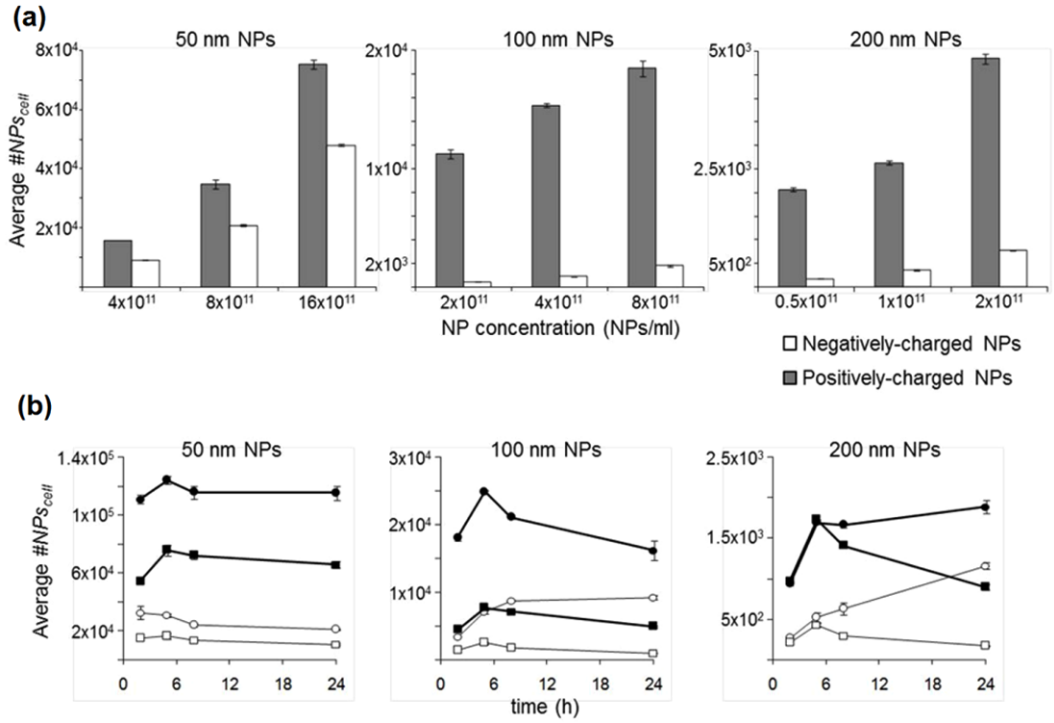

Figure 5. Quantitative measures of cellular uptake of negatively and positively charged NPs of different sizes, at different exposure concentrations. (a) Comparative uptake after 24 h NP incubation. Gray bars represent positively charged NPs; white bars represent negatively charged NPs. (b) Time course of cellular uptake of two different concentrations of positive (circles) and negative (squares) NPs. Cells were collected and analyzed after 2, 5, 8 and 24 h of exposure to 4×10^{11} (○; □) and 16×10^{11} (●; ■) 50 nm NPs ml^{-1}; 1×10^{11} (○), 4×10^{11} (●; □) and 16×10^{11} (■) 100 nm NPs ml^{-1} or 0.125×10^{11} (○), 0.5×10^{11} (●; □) and 2×10^{11} (■) 200 nm NPs ml^{-1}.

4. Conclusion

A method for quantitative evaluation of the cellular uptake of polymer NPs has been assessed based on parallel measures through three independent experimental platforms, whose results were integrated, overcoming their individual limitations. Monodispersed and fluorescent NPs, with RhB dye covalently bonded to the NPs, were produced with different and controlled sizes (50, 100 and 200 nm) and surface charges. For each type of polymer NP a simple and reproducible linear relationship had been established between the number of NPs, the molecules of RhB per NP and the relative fluorescence detected by the microplate reader. Taking into account the absolute number of cells, measured independently through a Coulter counter, a quantitative relationship was found between plate fluorimetry measures and average cell fluorescence measured by flow cytometer. This enabled us to calibrate the flow cytometric fluorescence scale and consequently to evaluate the number of NPs internalized in individual cells. The absolute NP quantification can be correlated to additional parameters measurable by flow cytometry, allowing us to take measures insensitive to the effects of aggregates of NPs and dead cells, which instead, when not negligible, would affect the bulk measure by plate fluorimetry. On the other hand, flow cytometry measures the overall fluorescence emitted by individual cells, but cannot detect NP localization inside or on the external membrane of the cells. For this reason the quantification achieved by flow cytometry is complemented with localization studies by imaging (live or confocal) techniques, in particular to exclude significant contributions of externally bound NPs.

The developed procedure has been applied to compare the uptake of various NPs as a function of their size (50–200 nm), surface charge (−40–40 mV) and concentration (10^{10}–10^{12} NPs ml^{-1}) into 4T1 cells. For all the NPs considered in this work, a fast increase of RhB-associated cellular fluorescence was observed a few minutes after NP exposition, with clear fluorescent spots in the perinuclear region. The perinuclear localization is typical of late endocytic organelles [28], suggesting that NPs were internalized via endocytic pathways. Quantitative kinetic measurements indicated that the uptake process reached a maximum in 2–5 h, and then stabilized within 24 h at a somewhat lower plateau value. While the uptake/efflux of smaller NPs (50 nm) was less dependent on the charge, it was crucial for larger NPs: 100 and 200 nm positively charged NPs had the highest cellular uptake and were strongly retained inside the cells, while uptake of negatively charged NPs was at least an order of magnitude lower and efflux was rapid after NP washout. The higher uptake of positively charged NPs was expected, in consideration of the attraction exerted by the negatively charged cytoplasmic membrane of the cells. Size-dependence of the efflux of NPs has also been reported in the literature [29]. However, the biophysical and molecular mechanisms driving NP uptake/efflux are far from being

completely disclosed, and the literature is controversial in this regard (e.g. [30]).

Although these conclusions are restricted to the cells and the NPs considered here, the procedure is of general validity and can be easily applied to other NP systems, stable in biological media and with a fluorescent dye covalently linked to the NPs themselves. The requirement of experimental techniques commonly available in biomedical research laboratories assures a potential broad application of the proposed method with any kind of fluorescent NP, with a known amount of a stably loaded fluorochrome, allowing a quantification of the uptake process with unprecedented performance and versatility.

Acknowledgment

We acknowledge support from the AIRC Special Program Molecular Clinical Oncology '5 per mille'.

References

[1] Brigger I, Dubernet C and Couvreur P 2002 *Adv. Drug Deliv. Rev.* **54** 631–51
[2] Bartlett D W, Su H, Hildebrandt I J, Weber W A and Davis M E 2007 *Proc. Natl Acad. Sci. USA* **104** 15549–54
[3] Lorenz M R, Holzapfel V, Musyanovych A, Nothelfer K, Walther P, Frank H, Landfester K, Schrezenmeier H and Mailander V 2006 *Biomaterials* **27** 2820–8
[4] dos Santos T, Varela J, Lynch I, Salvati A and Dawson K A 2011 *Small* **7** 3341–9
[5] Lorenz S, Hauser C P, Autenrieth B, Weiss C K, Landfester K and Mailänder V 2010 *Macromol. Biosci.* **10** 1034–42
[6] Smith P J, Giroud M, Wiggins H L, Gower F, Thorley J A, Stolpe B, Mazzolini J, Dyson R J and Rappoport J Z 2012 *Int. J. Nanomed.* **7** 2045–55
[7] Cho E C, Zhang Q and Xia Y 2011 *Nature Nanotechnol.* **6** 385–91
[8] Cho E C, Xie J W, Wurm P A and Xia Y N 2009 *Nano Lett.* **9** 1080–4
[9] Chithrani B D, Ghazani A A and Chan W C 2006 *Nano Lett.* **6** 662–8
[10] Ferrari R, Yu Y, Morbidelli M, Hutchinson R A and Moscatelli D 2011 *Macromolecules* **44** 9205–12
[11] Ferrari R, Yu Y, Lattuada M, Storti G, Morbidelli M and Moscatelli D 2012 *Macromol. Chem. Phys.* **213** 2012–8
[12] Norakankorn C, Pan Q M, Rempel G L and Kiatkamjornwong S J 2009 *J. Appl. Polym. Sci.* **113** 375–82
[13] Dossi M, Ferrari R, Dragoni L, Martignoni C, Gaetani P, D'Incalci M, Morbidelli M and Moscatelli D 2013 *Macromol. Mater. Eng.* **298** 730–9
[14] Cova L *et al* 2013 *Nanotechnology* **24** 245603
[15] Musyanovych A, Dausend J, Dass M, Walther P, Mailander V and Landfester K 2011 *Acta Biomater.* **7** 4160–8
[16] Shen Z L and Andersson S B 2011 *IEEE Trans. Control Syst. Technol.* **19** 1269–78
[17] Salvati A, Aberg C, dos Santos T, Varela J, Pinto P, Lynch I and Dawson K A 2011 *Nanomedicine* **7** 818–26
[18] Kim J A, Aberg C, Salvati A and Dawson K A 2012 *Nature Nanotechnol.* **7** 62–8
[19] Lee R J and Low P S 1994 *J. Biol. Chem.* **369** 3198–204
[20] Massignani M, LoPresti C, Blanazs A, Madsen J, Armes S P, Lewis A L and Battaglia G 2009 *Small* **5** 2424–32
[21] LoPresti C *et al* 2011 *ACS Nano* **5** 1775–84
[22] Summers H D, Brown M R, Holton M D, Tonkin J A, Hondow N, Brown A P, Brydson R and Rees P 2013 *ACS Nano* **7** 6129–37
[23] Zucker R M, Massaro E J, Sanders K M, Degn L L and Boyes W K 2010 *Cytometry* A **77A** 677–85
[24] Sajjadi S and Yianneskis M 2010 *Polym. React. Eng.* **11** 715–36
[25] Lesniak A, Campbell A, Monopoli M P, Lynch I, Salvati A and Dawson K A 2010 *Biomaterials* **31** 9511–8
[26] Desai M P, Labhasetwar V, Walter E, Levy R J and Amido G L 1997 *Pharm. Res.* **14** 1568–73
[27] Mailander V and Landfester K 2009 *Biomacromolecules* **10** 2379–400
[28] Tao K, Fang M, Alroy J and Sahagian G G 2008 *BMC Cancer* **8** 228
[29] Chithrani B D and Chan W C W 2007 *Nano Lett.* **7** 1542–50
[30] Iversen T G, Skotland T and Sandvig K 2011 *Nano Today* **6** 176–85